

MSTSL: Multi-Sensor Based Two-Step Localization in Geometrically Symmetric Environments

Zhenyu Wu¹, Yufeng Yue², Mingxing Wen¹, Jun Zhang¹, Guohao Peng¹, and Danwei Wang¹, *Fellow, IEEE*

Abstract—Symmetric environment is one of the most intractable and challenging scenarios for mobile robots to accomplish global localization tasks, due to the highly similar geometrical structures and insufficient distinctive features. Existing localization solutions in such scenarios either depend on pre-deployed infrastructures which are expensive, inflexible, and hard to maintain; or rely on single sensor-based methods whose initialization module is incapable to provide enough unique information. Thus, this paper proposes a novel Multi-Sensor based Two-Step Localization framework named MSTSL, which addresses the problem of mobile robot global localization in geometrically symmetric environments by utilizing the measured magnetic field, 2-D LiDAR, and wheel odometry information. The proposed system mainly consists of two steps: 1) Magnetic Field-based Initialization, and 2) LiDAR-based Localization. Based on the pre-built magnetic field database, multiple initial hypotheses poses can firstly be determined by the proposed two-stage initialization algorithm. Then, utilizing the obtained multiple initial hypotheses, the robot can be localized more accurately by LiDAR-based localization. Extensive experiments demonstrate the practical utility and accuracy of the proposed system over the alternative approaches in real-world scenarios.

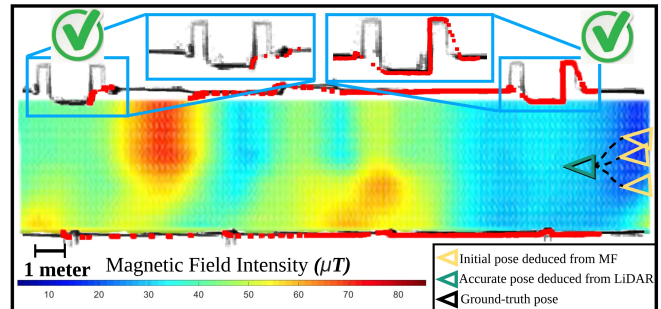
I. INTRODUCTION

Symmetric environments, such as office corridors and carparks, remain as critical and intractable scenarios for mobile robot to perform global localization tasks due to the highly similar geometrical structures and lack of distinctive features [1]–[9]. It is challenging to accomplish the initialization step or to restore the state of the kidnapped robot. Current localization solutions in such environments either count on pre-mounted infrastructures such as artificial landmarks, wireless beacons, guiding tapes, and QR-codes; or lean upon onboard sensors such as LiDAR, camera, and magnetic sensor (i.e. magnetometer). On the one hand, the infrastructure-dependent methods are neither credible nor scalable. Moreover, the costs of deploying and maintaining the infrastructures are quite high [10]–[14]. On the other hand, most of the initialization modules of the single sensor-based global localization algorithms are incapable to collect enough distinctive information, thus the robot may fail to localize in such symmetric environments [2], [3], [6], [7].

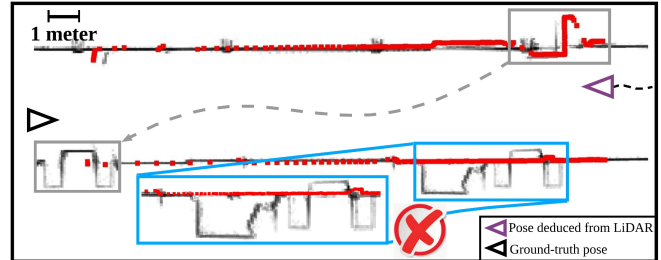
Magnetic field (MF) has prominent signatures at varying locations, which can be a viable alternative for localization due to its pervasive and distinctive characteristics [10]–[12], [15]–[20]. Researchers have demonstrated the feasibility of

¹Z. Wu, M. Wen, J. Zhang, G. Peng and D. Wang are with the School of Electrical and Electronic Engineering, Nanyang Technological University, Singapore 639798. E-mail: zhenyu002@e.ntu.edu.sg

²Y. Yue is with the School of Automation, Beijing Institute of Technology, Beijing 100081, China.



(a) Proposed MSTSL system—Successful



(b) LiDAR-based localization—Failed

Fig. 1. Localization in symmetric corridor environments, where background occupancy grid map is denoted in black, LiDAR measurements are depicted as red points, and robot trajectory is shown in black dashed line. (a) Proposed Multi-Sensor based Two-Step Localization (MSTSL) system—Successful. Colors of the MF denotes the MF integrated intensity. Multiple initial hypotheses poses are deduced by the MF-based initialization, which helps to disambiguate the similar structures. Then after a short movement, the accurate robot pose can be deduced by LiDAR-based localization; (b) LiDAR-based localization—Failed. The robot is susceptible to be mismatched to wrong places in such symmetric environments.

using the ambient MF alone for both indoor localization [10], [16], [18] and navigation [15], [17]. In addition, [16], [18] proved the stability of the disturbed MF over a long period of time. Apart from using MF alone, approaches such as [12], [21] proposed to fuse magnetic and visual sensors for indoor localization and achieved good accuracy. However, their methods vulnerable to illumination/viewpoint changes. Other approaches [22], [23] fuse magnetic sensing with Wi-Fi based methods to enhance localization performance, but they all need to deploy those inflexible infrastructures.

In addition to MF-based localization, 2-D LiDAR-based localization is widely adopted for mobile robot localization due to its high accuracy and robustness [2]–[7], [24]–[28]. Previous work including multiple hypothesis tracking-based [24], [25] and particle filter (PF)-based [2], [3], [26] methods were proposed to solve mobile robot global localization problem. In general, LiDAR-based localization approaches

operate well in regular environments with sufficient distinctive features [29], but they can be mismatched or even fail in symmetric environments due to the difficulty of disambiguating similar structures [2]–[7]. Thus, other approaches like the clustered PF [2], [3] and laser reflectivity-based strategy [6] were proposed to address the localization problem in symmetric or ambiguous environments. However, their proposed algorithms were only verified in small-scale environments and there was no explicit criterion for their localization error. Moreover, laser-based probabilistic methods [4], [5] were proposed to improve the localization performance in ambiguous environments. However, they have to decide where and how to deploy the artificial landmarks, which is still infrastructure-dependent and inflexible. In summary, we found that existing solutions have many limitations and the field still lacks of credible localization methods for geometrically symmetric environments [7], [20], which is the motivation for our research.

In this paper, we propose a novel Multi-Sensor based Two-Step Localization framework termed MSTSL, which incorporates a MF-based initialization module and a LiDAR-based localization module, to systematically tackle the problem of mobile robot localization in geometrically symmetric environments. A brief illustration comparing the proposed system with traditional LiDAR-based localization approach is shown in Fig. 1 as an example. The key novelty of this work is the mathematical modeling of the problem of multi-sensor based localization in symmetric environments and its probabilistic derivation. More specifically, this paper proposes the MSTSL framework to efficiently initialize and accurately localize the robot based on the measured MF, LiDAR, and wheel odometry information.

The rest of this paper is organized as follows: Section II overviews the proposed localization framework. Section III details the proposed MSTSL system. Section IV presents experimental verifications. Finally, Section V draws the conclusions.

II. SYSTEM OVERVIEW

The workflow of the proposed multi-sensor based two-step localization (MSTSL) system is shown in Fig. 2. This paper focuses on the 2-D global localization problem, where the robot pose \mathbf{x}_t at time step t can be denoted as a random variable $\mathbf{x}_t = [x, y, \psi]^T \in \mathbb{R}^2 \times \mathbb{S}$.

In the proposed system, the initial robot poses \mathbf{x}_i are introduced as the hidden variables to enhance the robot localization performance, which can be derived by the initialization step by utilizing both the MF information \mathbf{B} and LiDAR information \mathbf{L} . Given the independent sensor observations $\mathbf{z} = [\mathbf{z}_i, \mathbf{z}_l]^T = [\mathbf{z}_i^B, \mathbf{z}_i^L, \mathbf{z}_l^L]^T$, control input \mathbf{u}_l , and the pre-built map $\mathbf{M} = [\mathbf{m}^B, \mathbf{m}^L]^T$, the problem of mobile robot global localization in geometrically symmetric environments can be formulated as the estimation of the joint

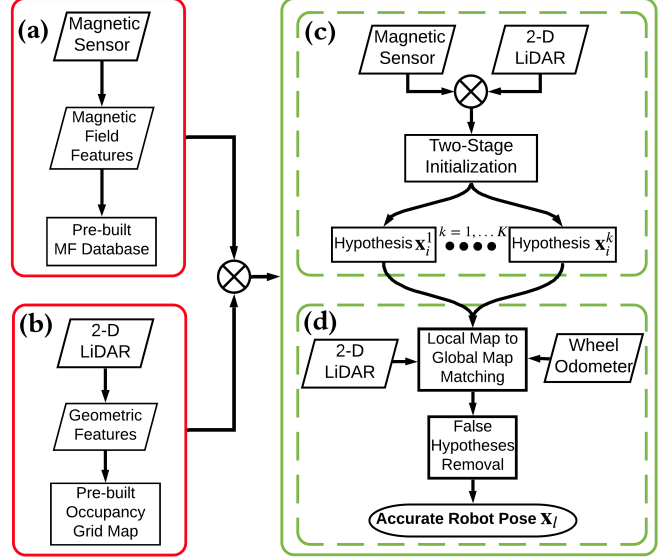


Fig. 2. Flowchart of the proposed MSTSL system. The whole system is divided into the *Offline Phase* (shown in red) and the *Online Phase* (shown in green). *Offline Phase* consists of two modules: (a) Collect MF data and build MF database; (b) Extract geometric features and build occupancy grid map (OGM). *Online Phase* consists of two steps: (c) MF-based Initialization. (d) LiDAR-based Localization.

probabilistic distribution denoted as:

$$p(\mathbf{x}_l, \mathbf{x}_i | \mathbf{z}_i, \mathbf{z}_l, \mathbf{u}_l, \mathbf{M}) = \underbrace{\sum_{k=1}^K p(\mathbf{x}_i^k | \mathbf{z}_i^k, \mathbf{m}^B)}_{\text{Initialization}} \underbrace{p(\mathbf{x}_l | \mathbf{x}_i^k, \mathbf{z}_l^L, \mathbf{u}_l^k, \mathbf{m}^L)}_{\text{Localization}} \quad (1)$$

where $k \in [1, K]$ denotes the k -th hypothesis pose and K denotes the top K robot hypotheses poses selected with high MF matching probability. $\mathbf{z}_i = [\mathbf{z}_i^B, \mathbf{z}_i^L]^T$ and $\mathbf{z}_l = \mathbf{z}_l^L$ denote the sensor observations of the initialization step and LiDAR-based localization step, respectively. \mathbf{m}^B and \mathbf{m}^L denote the MF database and occupancy grid map (OGM) built in the *Offline Phase*, respectively.

A. Magnetic Field-based Initialization

First of all, we look at the initial pose probabilistic distribution $p(\mathbf{x}_i^k | \mathbf{z}_i^k, \mathbf{m}^B)$, which is the first term on the right-hand side of Eq.(1). The objective of the MF-based initialization is to infer the initial hypothesis pose \mathbf{x}_i^k . By following the Bayesian theorem, it can be derived as:

$$p(\mathbf{x}_i^k | \mathbf{z}_i^k, \mathbf{m}^B) = \eta_i p(\mathbf{x}_i^k) p(\mathbf{z}_i^k | \mathbf{x}_i^k, \mathbf{m}^B) \quad (2)$$

where η_i is the normalization constant, term $p(\mathbf{x}_i^k)$ and $p(\mathbf{z}_i^k | \mathbf{x}_i^k, \mathbf{m}^B)$ are the prior estimation and observation model, respectively. In order to specify the initialization, prior information can be incorporated to evaluate the posterior. If no prior information is available, we assume $p(\mathbf{x}_i^k)$ to be a uniform distribution [1]. For the observation model, details are discussed in Section III-A.3.

B. LiDAR-based Localization

For the LiDAR-based robot pose inference, we elaborate the second term on the right-hand side of Eq.(1). The objective of the LiDAR-based localization is to estimate the accurate robot pose \mathbf{x}_l^k , which can be denoted by applying Bayesian theorem and Markov property as:

$$p(\mathbf{x}_l^k | \mathbf{x}_i^k, \mathbf{z}_l^k, \mathbf{u}_l^k, \mathbf{m}^L) = \eta_l p(\mathbf{x}_l^k | \mathbf{x}_i^k, \mathbf{u}_l^k) p(\mathbf{z}_l^k | \mathbf{x}_l^k, \mathbf{m}^L) \quad (3)$$

where η_l is a normalization constant. $p(\mathbf{x}_l^k | \mathbf{x}_i^k, \mathbf{u}_l^k)$ and $p(\mathbf{z}_l^k | \mathbf{x}_l^k, \mathbf{m}^L)$ are the motion model and observation model of the LiDAR-based localization step, respectively. The relative poses to the initial hypotheses poses are estimated by the proposed local map to global map matching. In the end, the accurate robot pose can be obtained after removing the false hypotheses. The detailed procedure of LiDAR-based localization is presented in Section III-B.

III. MULTI-SENSOR BASED TWO-STEP LOCALIZATION

The proposed MSTSL system consists of two modules: 1) MF-based initialization; 2) LiDAR-based localization. Details are presented below.

A. Magnetic Field-based Initialization

1) **Magnetic Field Properties:** Assuming the ambient MF is time-stationary [10], [16], [18], the ambient MF can be modeled as a 3-D vector $\mathbf{B} = [B^x, B^y, B^z]^T \in \mathbb{R}^3$ within the Cartesian coordinate system, where B^x , B^y , and B^z are the three orthogonal components representing intensities reported in microtesla (μT). The measured B^x is always in the same direction with the heading of the IMU/magnetometer [10], [16]. The Earth MF sets a background for the ambient MF, but anomalies caused by ferromagnetic objects, such as steels, electrical and electronic devices, deflect the Earth MF thus making the ambient MF unique at the local environment.

2) **Magnetic Field Modeling:** It is essential to interpolate and build the MF database \mathbf{m}^B due to the limited measurement range of the magnetometer. Different MF modeling methods are implemented, such as the fingerprints (FP)-based [7], [12], bilinear interpolation (BI)-based [16], [23], and Gaussian Process regression (GPR)-based [19], [22]. In our framework, GPR-based [19] approach is utilized due to its prominent accuracy and probabilistic derivation. Firstly, the MF vector at every 5cm interval along the robot survey trajectory is collected as the fingerprint. It is impractical for the robot to collect the MF fingerprints on all directions at each location. Thus, the mobile robot is teleoperated on different desired routes which are along the trajectories parallel to the straight borderline of the environments to record the MF fingerprints of two directions (0° and 180°).

Let $F = \{(\mathbf{p}_1, q_1), \dots, (\mathbf{p}_n, q_n)\}$ be a set of training samples chosen from the measured MF fingerprints, where \mathbf{p}_i and q_i denote the 2-D location vector and the corresponding 1-D magnetic intensity $B^x/B^y/B^z$. A GPR estimates posterior distributions over the model function $f(\mathbf{p})$ from training data F . The model function can be denoted as: $f(\mathbf{p}) \sim \mathcal{GP}(m(\mathbf{p}), k(\mathbf{p}, \mathbf{p}'))$, where $m(\mathbf{p}) \triangleq \mathbb{E}[f(\mathbf{p})]$ is the mean function, $k(\mathbf{p}, \mathbf{p}') \triangleq \mathbb{E}[(f(\mathbf{p}) - m(\mathbf{p}))(f(\mathbf{p}') - m(\mathbf{p}'))]$

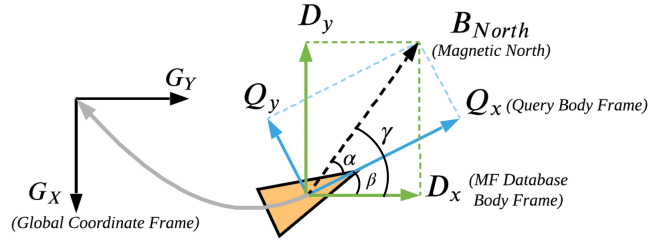


Fig. 3. Coordinates transformation relationship of the proposed two-stage initialization algorithm. The main target is to find the transformation relationship between the query body frame \mathbf{Q} (denoted in blue) and the global coordinate frame \mathbf{G} (denoted in black), where the MF database body frame \mathbf{D} (denoted in green) functions as the medium.

is the covariance function (where Gaussian Kernel is commonly chosen), and $\mathbb{E}[\cdot]$ is the expectation operator. Our objective is to predict the posterior distributions over $f(\mathbf{p})$ at an arbitrary query location \mathbf{p}_* . Thereby, the standard GPR equations [30] were applied to infer the mean μ and covariance matrix \mathbf{K} . A detailed discussion of the GPR algorithm is out of the scope of this paper, thus we refer the reader to [30]. Eventually, we define the MF database with a grid size of $5\text{cm} \times 5\text{cm}$ and the posterior distribution of each grid is calculated by three independent GPRs. Each grid cell of the MF database contains the 3-D MF vector, 2-D locations, and robot body frame.

3) **Two-Stage Initialization Algorithm:** In order to address the initialization problem of the mobile robot localization especially in geometrically symmetric environments, we propose the two-stage initialization algorithm, where the coordinates transformation relationship of the proposed algorithm is shown in Fig. 3. The proposed algorithm can be decomposed into two stages: 1) Location Determination; 2) Orientation Determination. Details of these two stages are elaborated in the following parts.

As aforementioned in Section III-A.2, the MF fingerprints of only two directions (0° and 180°) are collected. Thus, the robot needs to rotate by angle β to be parallelly aligned with the environment then MF-based matching can be implemented. We utilize the first frame of laser scan to estimate the angle β between heading direction Q_x and D_x . First of all, we transform the first frame of the laser scan into 2-D point clouds and implement the RANSAC algorithm [31] to fit the line, due to the reason that majority of the symmetric environments contains sufficient line configurations. Then we choose the line with the most inliers as the target line with known β . Eventually, we command the robot to rotate by β to align it with the fitted line.

a) **Stage 1: Location Determination:** After adjustment of the robot initial orientation, we can then match the current measured MF data \mathbf{D}_t with the pre-built MF database. For the \mathbf{Q} to \mathbf{D} rotation part shown in Fig. 3, we define $\alpha = \tan^{-1}(|Q_y|/|Q_x|)$ as the angle between Q_x and B_{North} and define $\gamma = \tan^{-1}(|D_y|/|D_x|)$ as the angle between D_x and B_{North} . Given that MF data at nearby locations may have similar values and considering the uncertainties, the top K hypotheses locations are selected according to their probabilities. In our framework, we utilize multivariate

Gaussian probability density function [19], [22] as the observation model $p(\mathbf{z}_i^k | \mathbf{x}_i^k, \mathbf{m}^B)$ in Eq. (2) for the GPR-based method. Regarding the FP-based and BI-based approaches, we utilize the k -NN algorithm embedded with Euclidean distance metric to select the K nearest locations.

b) Stage 2: Orientation Determination: Since we have deduced the i -th initial hypothesis location and corresponding MF database body frame \mathbf{D} in the previous stage, it is obvious that the origins of MF database body frame \mathbf{D} and global coordinate frame \mathbf{G} coincide with each other as shown in Fig. 3. Then for the orientation determination part, the heading of the i -th initial hypothesis body frame \mathbf{D}^i with respect to the \mathbf{G} can be expressed as a rotation matrix ${}^G R^i$ which satisfies $\mathbf{G} = {}^G R^i \cdot \mathbf{D}^i$. The angle ϕ and unified axis \mathbf{a} of the rotation are derived as: $\phi_i = \arccos((\mathbf{D}^i \cdot \mathbf{G}) / (\|\mathbf{D}^i\| \|\mathbf{G}\|))$; $\mathbf{a}_i = (\mathbf{D}^i \times \mathbf{G}) / (\|\mathbf{D}^i \times \mathbf{G}\|)$. Since the robot is assumed to be moving in parallel with the straight-line environmental configurations, we can divide the robot orientation θ determination problem into four cases as follows:

$$\theta = \begin{cases} 0, & \text{if } \phi_i = 0 \\ -\pi, & \text{if } \phi_i = \pi \\ -\frac{\pi}{2}, & \text{if } \phi_i = \frac{\pi}{2} \text{ and } \mathbf{a}_i \text{ pointing upwards} \\ \frac{\pi}{2}, & \text{if } \phi_i = \frac{\pi}{2} \text{ and } \mathbf{a}_i \text{ pointing downwards} \end{cases} \quad (4)$$

B. LiDAR-based Localization

Given the multiple initial hypotheses poses deduced from the previous initialization module, the goal of the proposed LiDAR-based localization module is to optimally match a current local map with a global reference map and find the accurate coordinates transformation. Firstly, laser range points are projected into 2-D grid cells. 2-D SLAM methods *Hector-SLAM* [27] and *Cartographer* [28] were utilized to build the OGM \mathbf{m}^L , and obtain the corresponding submaps $M_{G,a}$. To ensure successful localization, the mobile robot will start from \mathbf{x}_i^k and move to \mathbf{x}_l^k to observe the environment until it has successfully localized itself. Hence, the motion model $p(\mathbf{x}_l^k | \mathbf{x}_i^k, \mathbf{u}_l^k)$ in Eq. (3) can be denoted as:

$$\begin{cases} x_l^k = x_i^k + \Delta d_l^k \cos \theta_i^k \\ y_l^k = y_i^k + \Delta d_l^k \sin \theta_i^k \\ \theta_l^k = \theta_i^k + \Delta \theta_l^k \end{cases} \quad (5)$$

where $\mathbf{u}_l^k = [\Delta d_l^k, \Delta \theta_l^k]^T$ depicts the translational and rotational movements measured by wheel encoders from the k -th initial hypothesis state \mathbf{x}_i^k to final state \mathbf{x}_l^k .

In our method, the incoming laser scans with the moving robot are repeatedly aligned with the local map coordinate frames by a iterative process to build the local map of the k -th hypothesis pose $M_{L,k}$. We assume that each local map contains n small grid cells as $M_{L,k} = \{\langle m_{L,k}^{(1)}, \dots, m_{L,k}^{(n)} \rangle | n = 1, \dots, N\}$, where $m_{L,k}^{(n)}$ is a grid cell in $M_{L,k}$. Similarly, the submap $M_{G,s}$ centered at robot pose \mathbf{x}_s (when building the OGM) based on the global coordinate frame is depicted as $M_{G,s} = \{\langle m_{G,s}^{(1)}, \dots, m_{G,s}^{(n)} \rangle | s =$

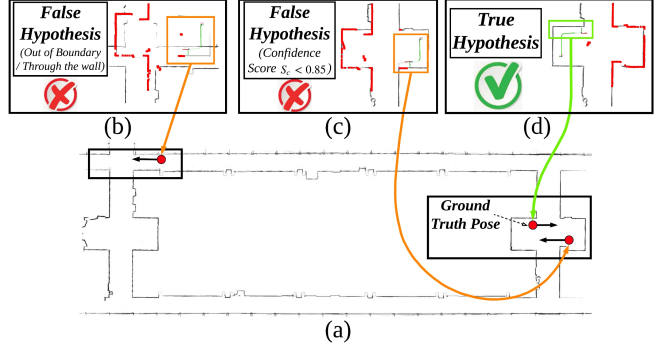


Fig. 4. The performance of the proposed MSTSL system in symmetric office corridor environment. LiDAR measurements are denoted as red points. (a) OGM of the corridor; (b) False hypothesis out of the boundary; (c) False hypothesis which confidence score is below threshold; (d) True hypothesis.

$1, \dots, S\}$. It is worth noting and apparent that $M_{L,k}$ and $M_{G,s}$ are of the same size. In the neighborhood of each initial hypothesis location (x_i^k, y_i^k) deduced by the MF-based initialization, each local map $M_{L,k}$ seeks to only search within $3\sigma_{x_i^k}$ confidence interval of x_i^k to reduce the computational load. Thereafter, we utilize the *Ceres*-based scan matcher [32] as the observation model $p(\mathbf{z}_l^k | \mathbf{x}_l^k, \mathbf{m}^L)$ in Eq. (3), where the accurate robot pose \mathbf{x}_l^k can be obtained when $M_{L,k}$ and $M_{G,s}$ achieve the best matching [33].

To achieve better localization accuracy, we evaluate the credibility of each obtained robot pose \mathbf{x}_l^k . Assuming that there are J^k laser points in the current laser scan of the k -th refined pose and each occupied grid cell hit by the laser point is assigned with a value of 1, we define the hypothesis confidence score S_j^k as: $S_j^k = (\sum_{j=1}^{J^k} P_j^k) / J^k$, where P_j^k denotes the number of hit occupied grid cells. An empirical threshold $S_j = 0.85$ is set to remove the false hypotheses. Besides, false hypotheses passing through the solid structure or beyond the map boundary, which indicates the robot is localized at unrealistic locations, are also removed. To make this issue more clear, one localization case of the proposed MSTSL system in geometrically symmetric office corridor environments is shown in Fig. 4. False hypotheses are shown in Fig. 4b and Fig. 4c, where they did not meet the requirement for the physical constraint or the confidence score. The credible true hypothesis is depicted in Fig. 4d.

IV. EXPERIMENTAL EVALUATION

A. Experimental Setup

Platform: The robot platform and robot body frame are demonstrated in Fig. 5a. A Xsens MTi-20 IMU is deployed at the central top frame and a Hokuyo UTM-30LX 2-D LiDAR is installed at the front.

MF Database & Occupancy Grid Map Building:

Two representative geometrically symmetric environments, one office corridor and another semi-indoor carpark, are selected for experiments. The robot was manually operated to go around the environment in both clockwise direction and counter-clockwise direction to collect the MF fingerprints of two directions (as aforementioned in Section III-A.2). We drove the robot (with known ground-truth initial

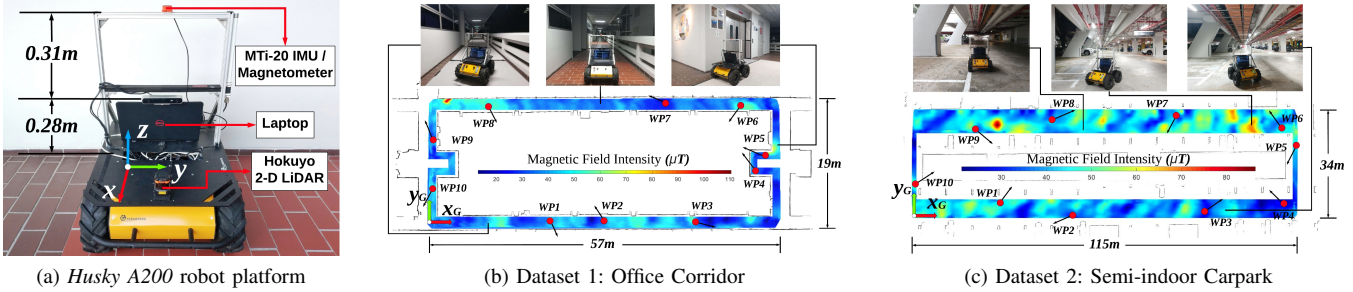


Fig. 5. (a) The IMU is installed on the central top frame, where it is 0.59m higher than the robot platform to avoid possible magnetic interference from other onboard sensors and motors; (b) and (c) visualize the fusion of MF databases and OGMS. Within each fused map, the color denotes the MF integrated intensity according to the scale shown in the center. Red dots represent randomly-selected waypoints (WPs, i.e. starting locations) and black arrows denote the initial heading direction of the robot.

pose) while implementing 2-D LiDAR-based particle filter algorithm [34] to acquire the locations of the magnetometer [19]. Then we utilized 2-D SLAM algorithms *Hector-SLAM* [27] and *Cartographer* [28] to build the OGMS, where a large number of them will be inaccurate and failed due to the symmetries and ambiguities of the environments [7]. We selected the most accurate and credible one OGM to utilize in our experiments. The resolution of the MF database and OGM were both set to 5cm. For the two datasets, the number of magnetic fingerprints used for the GPR learning were 67,238 and 118,688, respectively. The MF databases fused with the OGMS of the environments are visualized in Fig. 5b and Fig. 5c.

B. Evaluation Protocol

1) Methods for Comparison: As far as we know, no MF-based multi-sensor localization system is publicly available. Thus, the proposed MSTSL system is compared with three representative global localization algorithms, which are: 1) *AMCL* [26]; 2) *Cartographer* [28]; 3) *PF-Mag* [11]. For the LiDAR-based localization methods *AMCL* and *Cartographer*, default initial pose was found and set by their own algorithms. *PF-Mag* is a solely MF-based approach that encapsulates the particle filtering (PF) algorithm. Ten waypoints (WPs) were randomly selected in each dataset to evaluate the performance, where individual random tests were conducted ten times for each evaluated method of each WP. The ground-truth locations of the WPs were manually measured by a tape ruler.

2) Evaluation Criterions: For the evaluation of the MF-based initialization module, three algorithms, namely FP-based, BI-based and GPR-based approaches as aforementioned in Section III-A.2, are implemented and compared. In our experiments, we empirically set the criterion for the MF-based initialization error at 3.0m.

For the evaluation of mobile robot global localization performance, the following three criterions are selected: 1) Robustness; 2) Accuracy; and 3) Efficiency. Robustness is evaluated by the cumulative localization success rate, which is the average success rate over the ten WPs. Accuracy is measured by the cumulative distribution function (*CDF*) of the localization error. Besides, efficiency is assessed

by measuring the actual distance the robot has travelled to successfully localize itself (correct localization distance (*CLD*)). If the *CLD* is longer than 10.0m, we consider the localization as failed, thus eliminating the impact from those extreme outlier cases.

C. Experimental Evaluations

For the evaluation of the initialization step, the accuracy of three MF modeling methods over all WPs of each dataset is summarized in Table I. We list the average, standard deviation, minimum, maximum localization errors, respectively, and highlight the **best** results. Besides, we abbreviate the localization error and initialization success rate as “Loc.” and “Succ.”, respectively. We empirically determine the optimum K value for the two datasets as $K = 5$ and $K = 8$, respectively. If the mean localization error of the k -th initial location (x_i^k, y_i^k) is beyond the threshold 3.0m, then it is regarded as failed. The orientation adjustment done by the proposed two-stage initialization algorithm is abbreviated as “Ori. Adj.”, which is measured by the angle deviation from the fitted parallel line. The results clearly demonstrate that GPR-based method outperforms the other two approaches for modeling of the MF. Moreover, the low value of angle deviation also indicates the efficacy of the proposed two-stage initialization algorithm.

The office corridor environment is depicted in Fig. 5b. Firstly, the localization success rate is shown in Fig. 6a, where the proposed MSTSL system yields the highest rate of **96%** and the other approaches yield rates ranging from 0% to 63%. As for the semi-indoor carpark depicted in Fig. 5c,

TABLE I
INITIALIZATION RESULTS OF THE THREE MF MODELING METHODS

		FP		BI		GPR		Ori. Adj.
		Loc.	Succ.	Loc.	Succ.	Loc.	Succ.	
Dataset 1 ($K = 5$)	Ave.	1.232m	82%	1.15m	87%	0.852m	96%	1.23°
	Std.	0.721m		0.544m		0.502m		0.41°
	Min.	0.32m		0.26m		0.13m		0.3°
	Max.	4.75m		4.54m		3.97m		2.3°
Dataset 2 ($K = 8$)	Ave.	2.251m	76%	2.015m	82%	1.832m	93%	1.19°
	Std.	0.534m		0.362m		0.483m		0.35°
	Min.	1.35m		1.28m		1.2m		0.4°
	Max.	4.95m		4.76m		4.61m		2.8°

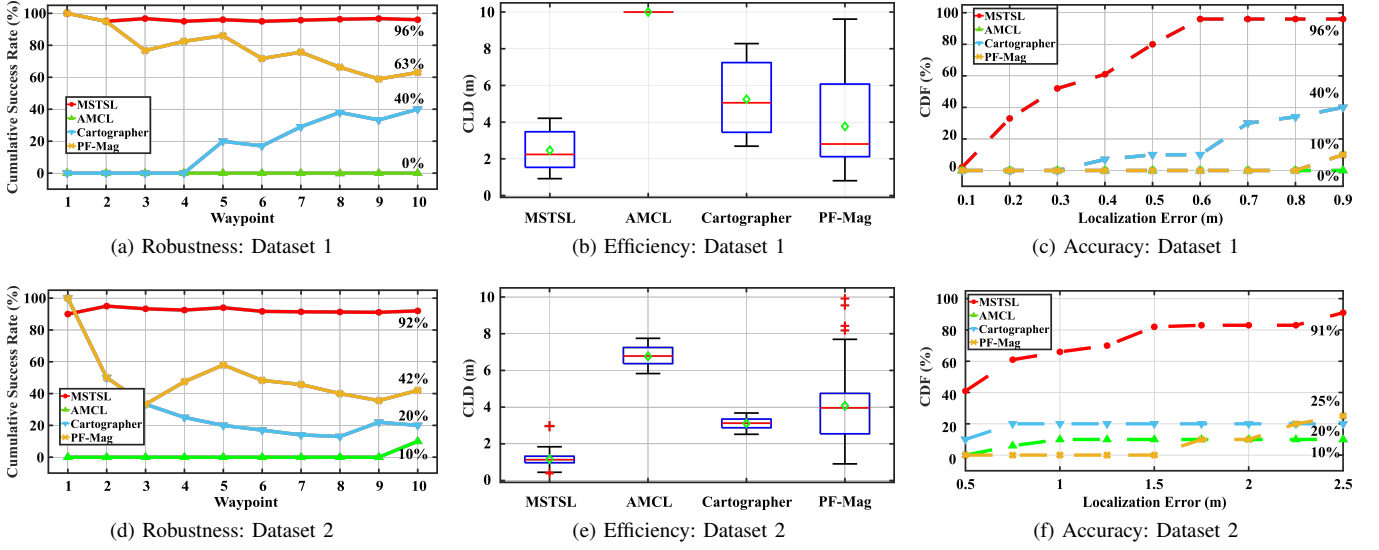


Fig. 6. **Left:** (a) and (d) are the cumulative localization success rate shown in line graph. **Middle:** (b) and (e) show the correct localization distance (*CLD*). The mean value, median value, and the outlier are depicted in green diamond, horizontal red line, red cross mark, respectively. **Right:** (c) and (f) are the Cumulative Distribution Function (*CDF*) plot of the localization error.

the localization success rate is shown in Fig. 6d, where the proposed method yields the highest rate of 92% and the other approaches yield rates ranging from 10% to 42%. Besides, it is obvious that the proposed method has the best *CLD* as shown in Fig. 6b and Fig. 6e, which demonstrates the superior efficiency of the proposed method. As for the accuracy evaluations shown in Fig. 6c and Fig. 6f, it is evident that *CDF* of the proposed method outperforms the three alternatives, achieving a 96% probability of 0.6m and a 80% probability of 1.5m for the two datasets, respectively.

In summary, it is observed from the experimental results that the proposed MSTSL system has greatly enhanced the localization robustness, efficiency, and accuracy, particularly in geometrically symmetric environments where prior MF-based initialization helps to disambiguate the similar structures. Moreover, we would like to mention that the proposed MSTSL system not only works in geometrically symmetric environments but also works in ordinary non-symmetric environments with sufficient unique features, where it is supposed to achieve better localization results than alternative global localization methods due to the distinctive information provided by the MF.

V. CONCLUSION

This paper presented a novel Multi-Sensor based Two-Step Localization framework named MSTSL, which significantly improved the performance of mobile robot localization in geometrically symmetric environments by leveraging the magnetic field (MF), LiDAR, and wheel odometry information. The proposed system mainly consists of MF-based initialization and LiDAR-based localization, where the introduction of MF information provides a robust and effective initialization approach for the mobile robot localization. Real-world experimental results indicate that the proposed MSTSL system has greatly enhanced the feasibility and

accuracy of localization in symmetric environments. For possible industrial applications, the proposed MSTSL system provides an inexpensive and promising solution for robot localization in warehouse environments. Future work will investigate algorithms to tightly couple the MF-based method with LiDAR-based method for addressing loop closure detection and SLAM problem.

REFERENCES

- [1] S. Thrun *et al.*, *Probabilistic robotics*. The MIT press, 2005.
- [2] A. Milstein *et al.*, “Robust global localization using clustered particle filtering,” in *AAAI/IAAI*, 2002, pp. 581–586.
- [3] Z. Liu *et al.*, “Mobile robots global localization using adaptive dynamic clustered particle filters,” in *2007 IEEE/RSJ International Conference on Intelligent Robots and Systems (IROS)*. IEEE, 2007, pp. 1059–1064.
- [4] D. Meyer-Delius *et al.*, “Using artificial landmarks to reduce the ambiguity in the environment of a mobile robot,” in *2011 IEEE International Conference on Robotics and Automation (ICRA)*. IEEE, 2011, pp. 5173–5178.
- [5] M. Beinhofer *et al.*, “Deploying artificial landmarks to foster data association in simultaneous localization and mapping,” in *2013 IEEE International Conference on Robotics and Automation (ICRA)*. IEEE, 2013, pp. 5235–5240.
- [6] D. Zhang *et al.*, “Robot localization under perceptual aliasing conditions based on laser reflectivity using particle filter,” in *2011 IEEE/SICE International Symposium on System Integration (SII)*. IEEE, 2011, pp. 90–95.
- [7] Z. Wu *et al.*, “Infrastructure-free global localization in repetitive environments: An overview,” in *IECON 2020 - 46th Annual Conference of the IEEE Industrial Electronics Society*. IEEE, 2020, pp. 626–631.
- [8] G. Peng *et al.*, “Semantic reinforced attention learning for visual place recognition,” in *2021 International Conference on Robotics and Automation (ICRA)*. IEEE, to be published, 2021.
- [9] Y. Yue and D. Wang, *Collaborative Perception, Localization and Mapping for Autonomous Systems*. Springer Nature, 2021, vol. 2.
- [10] M. Angermann *et al.*, “Characterization of the indoor magnetic field for applications in localization and mapping,” in *Indoor Positioning and Indoor Navigation (IPIN), 2012 International Conference on*. IEEE, 2012, pp. 1–9.
- [11] M. Frassl *et al.*, “Magnetic maps of indoor environments for precise localization of legged and non-legged locomotion,” in *2013 IEEE/RSJ International Conference on Intelligent Robots and Systems (IROS)*. IEEE, 2013, pp. 913–920.

- [12] Z. Liu *et al.*, “Fusion of magnetic and visual sensors for indoor localization: Infrastructure-free and more effective,” *IEEE Transactions on Multimedia*, vol. 19, no. 4, pp. 874–888, 2017.
- [13] X. Tang *et al.*, “Place recognition using line-junction-lines in urban environments,” in *2019 IEEE International Conference on Cybernetics and Intelligent Systems (CIS) and IEEE Conference on Robotics, Automation and Mechatronics (RAM)*. IEEE, 2019, pp. 530–535.
- [14] Y. Yue *et al.*, “Collaborative semantic understanding and mapping framework for autonomous systems,” *IEEE/ASME Transactions on Mechatronics*, to be published, 2020.
- [15] W. Kwon *et al.*, “Particle filter-based heading estimation using magnetic compasses for mobile robot navigation,” in *2006 IEEE International Conference on Robotics and Automation (ICRA)*. IEEE, 2006, pp. 2705–2712.
- [16] J. Haverinen and A. Kemppainen, “Global indoor self-localization based on the ambient magnetic field,” *Robotics and Autonomous Systems*, vol. 57, no. 10, pp. 1028–1035, 2009.
- [17] B. Gozick *et al.*, “Magnetic maps for indoor navigation,” *IEEE Transactions on Instrumentation and Measurement*, vol. 60, no. 12, pp. 3883–3891, 2011.
- [18] B. Li *et al.*, “How feasible is the use of magnetic field alone for indoor positioning?” in *Indoor Positioning and Indoor Navigation (IPIN), 2012 International Conference on*. IEEE, 2012, pp. 1–9.
- [19] N. Akai and K. Ozaki, “Gaussian processes for magnetic map-based localization in large-scale indoor environments,” in *2015 IEEE/RSJ International Conference on Intelligent Robots and Systems (IROS)*. IEEE, 2015, pp. 4459–4464.
- [20] Z. Wu *et al.*, “Magnetic-assisted initialization for infrastructure-free mobile robot localization,” in *2019 IEEE International Conference on Cybernetics and Intelligent Systems (CIS) and IEEE Conference on Robotics, Automation and Mechatronics (RAM)*. IEEE, 2019, pp. 518–523.
- [21] K. Wang *et al.*, “A simple and parallel algorithm for real-time robot localization by fusing monocular vision and odometry/AHRS sensors,” *IEEE/ASME Transactions on Mechatronics*, vol. 19, no. 4, pp. 1447–1457, 2014.
- [22] Y. Li *et al.*, “Using Wi-Fi/magnetometers for indoor location and personal navigation,” in *2015 International Conference on Indoor Positioning and Indoor Navigation (IPIN)*. IEEE, 2015, pp. 1–7.
- [23] Y. Shu *et al.*, “Magicol: Indoor localization using pervasive magnetic field and opportunistic WiFi sensing,” *IEEE Journal on Selected Areas in Communications*, vol. 33, no. 7, pp. 1443–1457, 2015.
- [24] P. Jensfelt and S. Kristensen, “Active global localization for a mobile robot using multiple hypothesis tracking,” *IEEE Transactions on Robotics and Automation*, vol. 17, no. 5, pp. 748–760, 2001.
- [25] K. O. Arras *et al.*, “Feature-based multi-hypothesis localization and tracking using geometric constraints,” *Robotics and Autonomous Systems*, vol. 44, no. 1, pp. 41–53, 2003.
- [26] D. Fox, “Adapting the sample size in particle filters through KLD-sampling,” *The International Journal of Robotics Research*, vol. 22, no. 12, pp. 985–1003, 2003.
- [27] S. Kohlbrecher *et al.*, “A flexible and scalable SLAM system with full 3D motion estimation,” in *2011 IEEE International Symposium on Safety, Security, and Rescue Robotics*. IEEE, 2011, pp. 155–160.
- [28] W. Hess *et al.*, “Real-time loop closure in 2D LIDAR SLAM,” in *2016 IEEE International Conference on Robotics and Automation (ICRA)*. IEEE, 2016, pp. 1271–1278.
- [29] Y. Yue *et al.*, “Collaborative semantic perception and relative localization based on map matching,” in *2020 IEEE/RSJ International Conference on Intelligent Robots and Systems (IROS)*. IEEE, 2020, pp. 6188–6193.
- [30] C. E. Rasmussen and C. K. Williams, *Gaussian Processes for Machine Learning*. The MIT Press, 2006.
- [31] M. A. Fischler *et al.*, “Random sample consensus: a paradigm for model fitting with applications to image analysis and automated cartography,” *Communications of the ACM*, vol. 24, no. 6, pp. 381–395, 1981.
- [32] S. Agarwal, K. Mierle *et al.*, “Ceres solver,” 2012. [Online]. Available: <http://ceres-solver.org/>
- [33] J. Xie *et al.*, “A real-time robust global localization for autonomous mobile robots in large environments,” in *2010 11th International Conference on Control Automation Robotics & Vision (ICARCV)*. IEEE, 2010, pp. 1397–1402.
- [34] S. Thrun *et al.*, “Robust monte carlo localization for mobile robots,” *Artificial intelligence*, vol. 128, no. 1-2, pp. 99–141, 2001.